Available online at www.sciencedirect.com

ScienceDirect

Ceramics International 40 (2014) 1545–1552

CERAMICS INTERNATIONAL

www.elsevier.com/locate/ceramint

Effect of annealing temperature on structural and optical properties of Mg-doped ZnO nanoparticles and their photocatalytic efficiency in alprazolam degradation

T.B. Ivetić[a,*], M.R. Dimitrievska[a], N.L. Finčur[b], Lj.R. Đačanin[a], I.O. Gúth[a], B.F. Abramović[b], S.R. Lukić-Petrović[a]

[a]Department of Physics, Faculty of Sciences, University of Novi Sad, Trg Dositeja Obradovića 4, 21000 Novi Sad, Serbia
[b]Department of Chemistry, Biochemistry and Environmental Protection, Faculty of Sciences, University of Novi Sad, Trg Dositeja Obradovića 3, 21000 Novi Sad, Serbia

Received 23 May 2013; received in revised form 6 July 2013; accepted 7 July 2013
Available online 13 July 2013

Abstract

Mg-doped ZnO nanocrystallites were prepared via conventional solid-state reaction when ZnO and MgO precursors were stoichiometrically mixed and heated at 700 °C, 900 °C and 1100 °C for 2 h in air atmosphere. Influence of annealing temperature on structural and optical properties of the obtained nanoparticles was investigated using X-ray diffraction, scanning electron microscopy, mercury intrusion porosimetry, Raman and UV–vis spectroscopy. The efficiency of Mg-doped ZnO water suspensions in the photocatalytic degradation of alprazolam, short-acting anxiolytic of the benzodiazepine class of psychoactive drugs, under UV irradiation was compared with efficiency of pure ZnO and TiO_2 Degussa P25.

Keywords: A. Powders: solid state reaction; B. Spectroscopy; D. ZnO; Photodegradation

1. Introduction

Environmentally friendly and inexpensive Mg-doped ZnO material system is being investigated for diverse applications which are mainly related to the band gap widening of ZnO by alloying with MgO. By changing the Mg-content, the direct band gap of the Mg-doped ZnO semiconductor could be adjusted from 3.37 eV to 7.8 eV [1]. Similar ionic radii of Zn^{2+} (0.60 Å) and Mg^{2+} (0.57 Å) enable formation of the solid solution despite the lattice mismatch between ZnO (hexagonal wurtzite: $a=3.25$ Å and $c=5.20$ Å) and MgO (cubic periclase: $a=4.24$ Å) structures. Solubility limit of MgO in ZnO is highly restricted (up to 4 at%) [2] and dependent upon the preparation conditions. Mg-doped ZnO is potentionaly attractive material to use in novel optoelectronic and nanoelectronic devices [1,3] and photocatalytic applications [3,4].

Pharmaceuticals are a large group of chemicals which are consumed in very high quantities throughout the world. These compounds are being introduced into the environment on a continuous basis and its continuous input and persistence to the water system may result in a potential risk for aquatic and terrestrial organisms. Until now, a vast group of pharmaceuticals has been found in the environment: analgetics, antibiotics, antiepileptics, β-blockers, antidepressants, anxiolytics, sedatives and contaceptives [5]. Benzodiazepines are widely consumed psychiatric pharmaceuticals and these compounds act on the central nervous system, having anxiolytic, sedative and hypnotic effects [5]. Calisto et al. investigated the relevance of photodegradation processes on the environmental persistence of four benzodiazepines (oxazepam, diazepam, lorazepam and alprazolam). Benzodiazepines were irradiated under simulated solar irradiation and lorazepam was shown to be quickly photodegradated by direct solar radiation, with a half-life time lower than 1 summer sunny day. Other three benzodiazepines oxazepam, diazepam and alprazolam showed to be highly resistant with half-life times of 4, 7 and 228 summer sunny days respectively [6].

Alprazolam (8-chloro-1-methyl-6-phenyl-4H-[1,2,4]triazole [4,3,-α]-[1,4]-benzodiazepine, CAS no. 28981-97-7, $C_{17}H_{13}ClN_4$,

*Corresponding author. Tel.: +381 21 4852826; fax: +381 21 459367.
E-mail address: tamara.ivetic@df.uns.ac.rs (T.B. Ivetić).

0272-8842/$ - see front matter © 2013 Elsevier Ltd and Techna Group S.r.l. All rights reserved.
http://dx.doi.org/10.1016/j.ceramint.2013.07.041

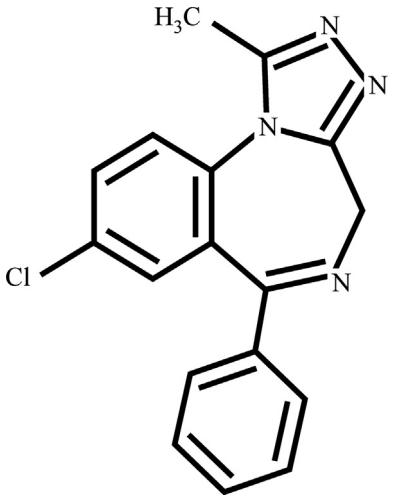

Fig. 1. Structural formula of alprazolam.

M_r=308.765, Fig. 1) is a benzodiazepine derived from 1,4-benzodiazepines of new generation. Alprazolam is extensively prescribed for its therapeutic application such as anxiolytics, anticonvulsant and antidepressant. It is used in the treatment of pathologies that imply anxiety disorders of chronic intensity as the social phobia and other psychosocial pathologies [7,8].

In this work, Mg-doped ZnO powders synthesized via simple solid-state reaction were structurally and optically characterized in an attempt to explain their photocatalytic efficiency differences in degradation of alprazolam. To the best of our knowledge, this is the first study of photocatalytic degradation of alprazolam.

2. Experimental procedures

2.1. Materials and characterization

The Mg-doped ZnO powder samples were obtained when starting ZnO (Sigma-Aldrich, purity 99.9%) and MgO (Centrohem, p.a.) were stoichiometrically mixed to achieve about 5% (w/w) of Mg-doping, in an agate mortar for 10 min and heated in furnace at 700 °C, 900 °C and 1100 °C for 2 h. X-ray diffraction was carried out using a Philips PW 1050 instrument, with Cu $K\alpha_{1,2}$ radiation, and a step scan mode of 0.02°/5 s in angular range 2θ=20–80°. A scanning electron microscope (SEM—JEOL JSM 6460LV) was used to investigate the morphology and microstructure of the samples.

The bulk density measurements were performed on a Macropore Unit 120 (Fisons Instruments). Total mercury intrusion volume (V_{tot}) and specific surface area (SSA) were performed on a Porosimeter 2000 (Fisons Instruments) within the pressure range from 1 to 2000 bar. All samples were dried in an oven at 110 °C during 16 h and additionally evacuated for 90 min at room temperature prior to analysis. Recording of intruded Hg volume vs. applied pressure values was obtained through an interface Milestone 100 Software System for PC. Additionally a Pascal Ver.1.05 software was used for calculation of bulk density (ρ_{bl}), V_{tot} and SSA.

The reflectance spectra were obtained for all samples using an Ocean Optics QE65000 High-sensitivity Fiber Optic Spectrometer, and in accordance with it the Kubelka–Munk function was estimated using a SpectraSuite Ocean Optics operating software. The Raman spectra of the samples were measured using the Centice MMS Raman spectrometer equipped with a CCD detector. A diode laser operating at 785 nm (1.58 eV) with power of 70 mW was used as the excitation source. All measurements were carried out at room temperature.

2.2. Measurements of photocatalytic activity

The photocatalytic activity of the Mg-doped ZnO powders was evaluated by the degradation of the solution of alprazolam (Sigma-Aldrich). The photocatalytic degradation was carried out in a cell described previously [9]. A 125 W high-pressure mercury lamp (Philips, HPL-N, emission bands in the UV region at 304, 314, 335 and 366 nm, with maximum emission at 366 nm), together with an appropriate concave mirror, was used as the radiation source.

Experiments were carried out using 20 mL of 0.03 mmol/L of alprazolam solution and the photocatalyst loading was 1.0 mg/mL. The aqueous suspension was sonicated (50 Hz) in dark for 15 min before illumination, to uniformly disperse the photocatalyst particles and attain adsorption equilibrium. The suspension thus obtained was thermostated at 25 ± 0.5 °C in a stream of O_2 (3.0 mL/min), and then irradiated. During irradiation, the mixture was stirred at a constant rate under continuous O_2 flow. Commercially available TiO_2 Degussa P25 (75% anatase and 25% rutile, specific area of 50 $m^2\,g^{-1}$, and average particle size about 20 nm, according to the producer's specification), was used for the purpose of comparison.

For the HPLC–DAD kinetic studies of alprazolam photodegradation, aliquots of 0.50 mL were taken from the reaction mixture at the beginning of the experiment and at regular time intervals. Aliquot sampling caused a maximum volume variation of ca. 10% in the reaction mixture. The suspensions containing photocatalyst were filtered through a Millipore (Milex-GV, 0.22 μm) membrane filter. After that, a 10-μL sample was injected and analyzed on HPLC—Shimadzu equipped with an Eclypse XDB-C18 column (150 mm × 4.6 mm i.d., particle size 5 μm, 25 °C). The UV/vis DAD detector was set at 222 nm (wavelength of alprazolam maximum absorption). The mobile phase (flow rate 1 mL/min) was a mixture of acetonitrile (ACN, 99.8%, J.T. Baker) and water (40:60, v/v), the water being acidified with 0.1% H_3PO_4 (85%, Sigma-Aldrich).

3. Results and discussion

3.1. Structural and optical characterization

The diffuse reflectance spectra of pure and Mg-doped ZnO powder samples obtained after annealing at 700 °C, 900 °C and 1100 °C were measured to investigate their optical properties.

The optical band gap energies E_g, were estimated from plots of $(F(R)h\upsilon)^2$ vs. photon energy $h\upsilon$ (Fig. 2), where $F(R)$ is the Kubelka–Munk function defined as $F(R)=(1-R)^2/2R$ and R is the measured diffuse reflectance [10]. Optical band gap energies obtained by extrapolation of $F(R)=0$ are shown in Table 1. ZnO and Mg-doped ZnO samples annealed at 700 °C have the absorption edge in the range 3.2–3.3 eV, which is usually reported for powder ZnO [11] (Table 1). Samples prepared at higher temperatures (presumably with larger particles) show characteristic red-shift in the absorption edge and optical band gap values below the reference [11].

Furthermore, small but obvious differences in optical properties between samples annealed at the same temperature were detected. When comparing optical band gap values of pure and Mg-doped ZnO samples annealed at the same temperature (Table 1), the blue shift indicates that Mg-doping affects the absorption edge due to Mg^{2+} incorporation into the ZnO lattice. Increase of the optical band gap energy with Mg-doping is commonly attributed to the so-called Moss–Burstein effect [1,12,13] caused by electrons generated by oxygen vacancies. When Mg^{2+} substitute the Zn^{2+}, because of the electro-negativity and ionic radius difference between Zn and Mg, the increase in oxygen vacancies and electron concentration appears. Lifting of the Fermi-level to the conduction band of the generated semiconductor caused by this carrier density increase arise in the optical band gap widening.

For further insight to the structural changes induced by Mg-doping at different annealing temperatures, the Mg-doped ZnO samples were investigated in detail using XRD and Raman spectroscopy (Figs. 3–6).

Fig. 3 shows the room temperature X-ray diffraction patterns of the Mg-doped ZnO sample annealed at different temperatures. The diffraction peaks for all Mg-doped ZnO samples match well with JCPDS Card (No. 05-0664) for hexagonal ZnO. The lattice parameters are important to determine whether Mg^{2+} have been embedded into the lattice of ZnO or not. Lattice constants a and c of wurtzite hexagonal ZnO structure were calculated [14] while the crystallite sizes were estimated using Debye Scherrer's equation

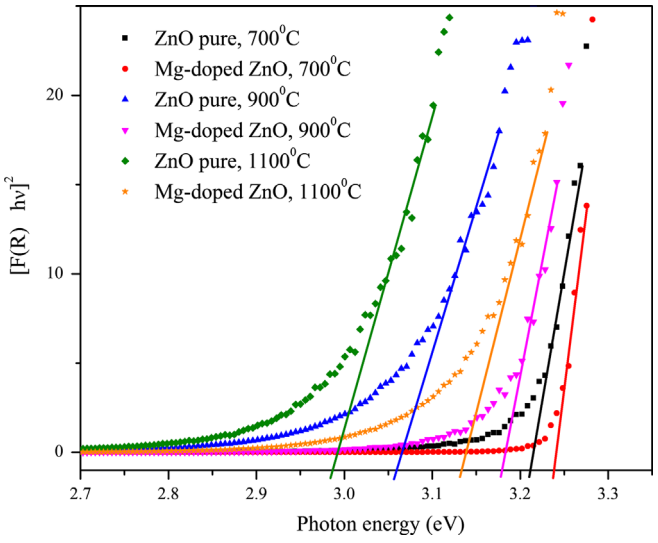

Fig. 2. Kubelka–Munk transformed reflectance spectra of pure ZnO and Mg-doped ZnO samples annealed at different temperatures.

Table 1
Optical band gap values of pure ZnO and the Mg-doped ZnO samples annealed at different temperatures.

Sample	Optical band gap (eV)		
	700 °C	900 °C	1100 °C
Pure ZnO	3.21	3.06	2.99
Mg-doped ZnO	3.24	3.18	3.13

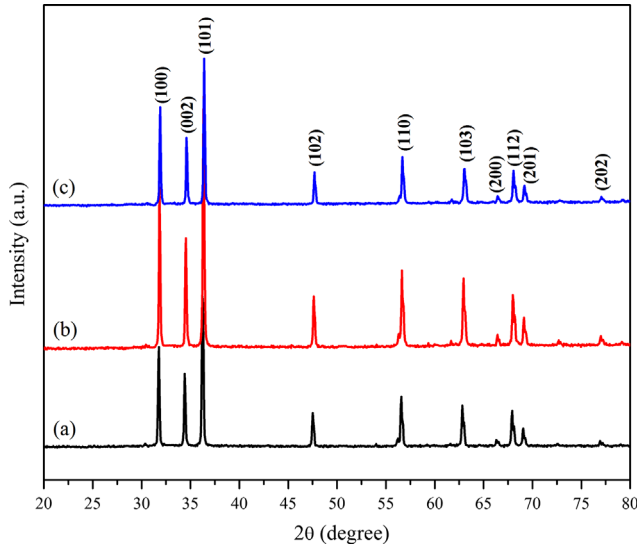

Fig. 3. XRD of Mg-doped ZnO sample annealed at: (a) 700 °C, (b) 900 °C and (c) 1100 °C.

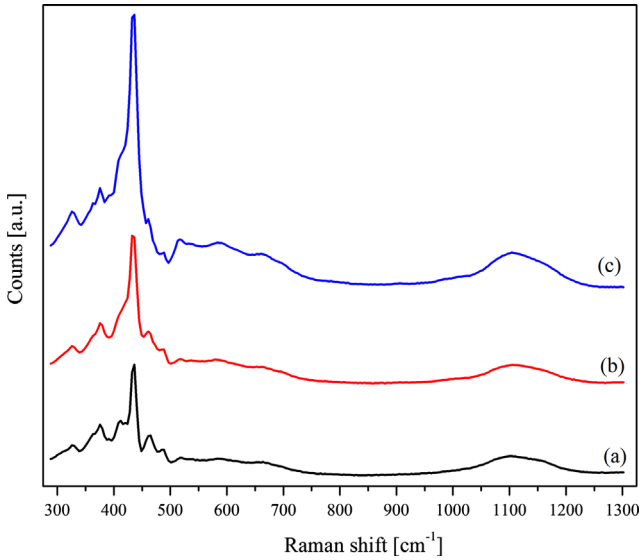

Fig. 4. Raman spectra of Mg-doped ZnO sample annealed at: (a) 700 °C, (b) 900 °C and (c) 1100 °C.

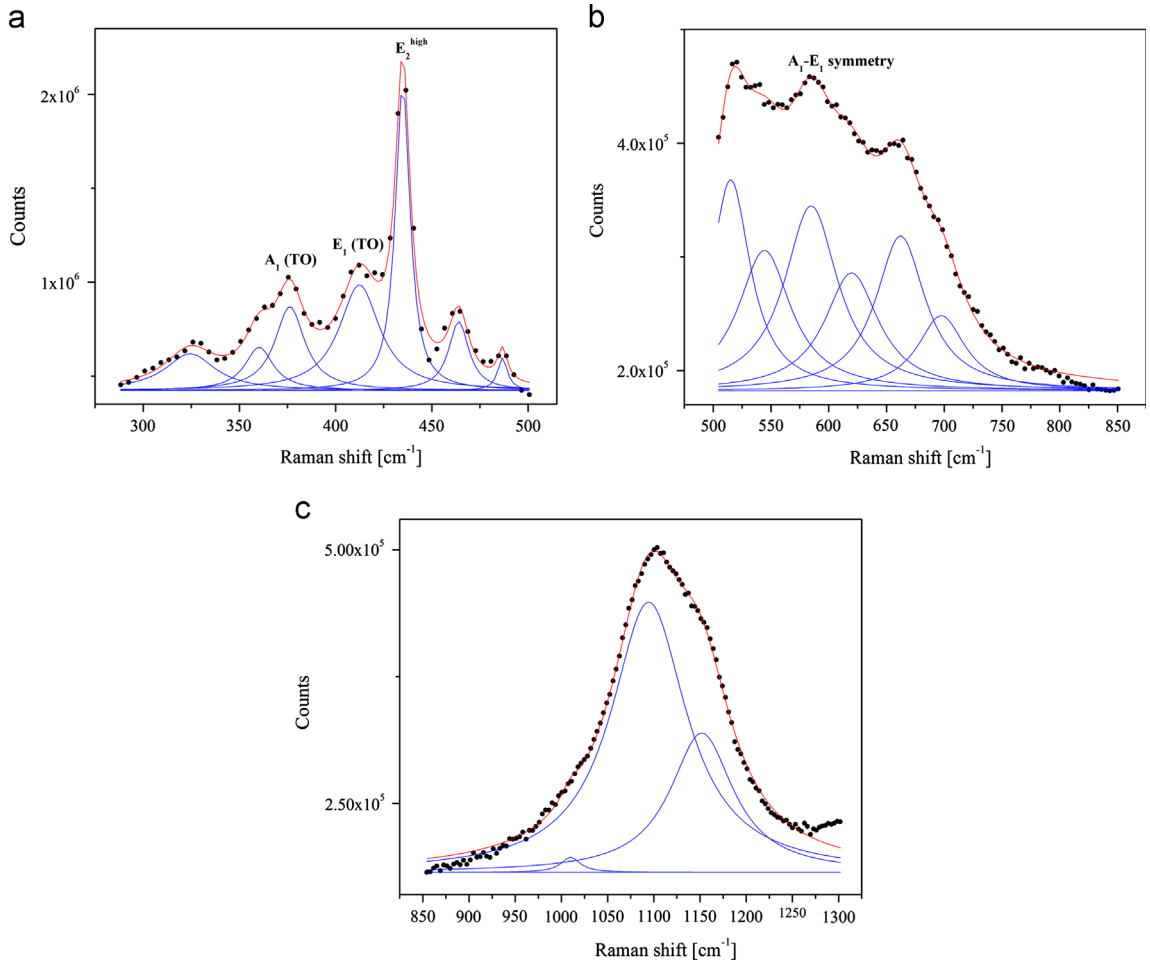

Fig. 5. Example of deconvoluted Raman spectrum (Mg-doped ZnO sample annealed at 700 °C): (a) 280–500 cm^{-1}; (b) 500–850 cm^{-1} and (c) 850–1300 cm^{-1} region (dots-experimental points, straight red line-fitted) with notation of the A_1 (TO), E_1 (TO), E_2^{high}, and E_1-A_1(LO) first-order ZnO Raman modes.

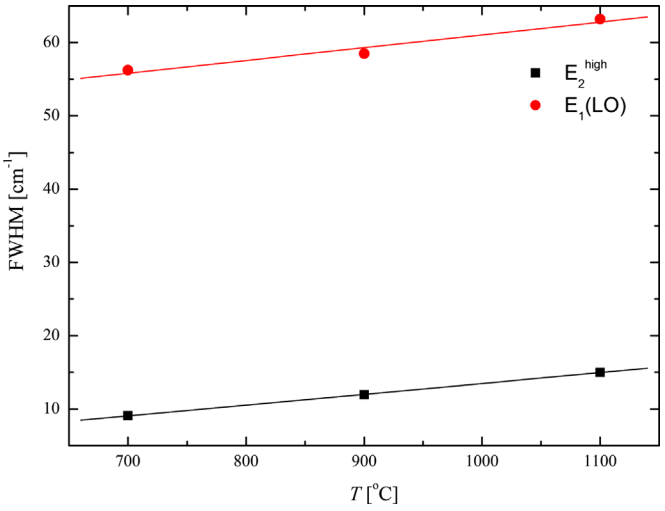

Fig. 6. FWHMs vs. annealing temperature for the E_2^{high} and E_1 (LO) modes in Mg-doped ZnO samples.

[15] by determining the line broadening of the (101) main intensity peak with PeakFit^{TM} v4.05 (SPSS Inc.) software package and are shown in Table 2.

The slight expansion of the lattice constants for the Mg-doped ZnO sample annealed at 700 °C compared to reference values (JCPDS Card no. 05-0664: $a=3.249$; $c=5.205$) indicates that Mg did not substitute Zn but it formed the interstitial Mg [12]. Similar a lattice constant for Mg-doped ZnO samples annealed at 900 °C and 1100 °C and slightly larger compression of c constant is expected for a Mg-substituted ZnO solid solution according to Vegard's law [1,16], as ionic radius of Mg^{2+} (0.057 nm) is smaller than Zn^{2+} (0.060 nm). This indicates Zn replacement with Mg in ZnO tetrahedral coordination for Mg-doped ZnO samples annealed at temperatures ≥900 °C.

Raman scatterings (Fig. 4) confirmed that synthesized Mg-doped ZnO samples have crystalline nature with hexagonal wurtzite structure but with obvious structural disorder induced by the preparation procedure and presence of impurities that will be discussed below.

The exact peak positions (frequency) and half-widths (FWHMs) of each band were determined by fitting the Lorentzian line shapes to the spectra. To achieve the most accurate deconvolution of the obtained Raman spectra each spectrum was divided into three parts and analyzed separately (Fig. 5). The intense narrow line at 435 cm^{-1} (E_2^{high} first-order ZnO Raman mode-associated with the vibration of oxygen atoms), which dominates the spectra, surely

indicates that these are the scatterings from the hexagonal modification of ZnO [17] with good crystallinity [18]. Wurtzite-type ZnO belongs to the space group C_{6v}^4 and optical phonons belong to the following irreducible representations: $\Gamma_{opt}=A_1+E_1+2E_2+2B_1$. The B_1 modes are silent, the A_1 and E_1 are polar modes and both Raman and infrared active, while E_2 are nonpolar and only Raman active [17]. Additionally, A_1 and E_1 optical phonons are split into transverse (TO) and longitudinal (LO) branches, while E_2 mode consists of low- and high-frequency phonons.

The E_1 (TO) and A_1 (TO) first-order Raman modes observed at ~412 cm^{-1} and ~376 cm^{-1}, respectively reflect the strength of the polar lattice bonds and their peak shift indicates a change in lattice constants. Two symmetry types of first-order Raman active LO modes: A_1 (LO) and E_1 (LO) occur depending on the experimental geometry [19]. As powders have tilted orientation the two LO modes are expected to interact and create one single mode of mixed A_1–E_1 symmetry known as quasi-LO mode, where E_1 (LO) frequency is expected to show blue shift while A_1 (LO) is almost unaffected by Mg-doping [19]. Nevertheless, as the A_1 (LO) was hard to resolve, we assume that the broad peak at ~584 cm^{-1} has mostly E_1 symmetry, and was assigned to E_1 (LO) mode (Table 3). Both A_1 (LO) and especially E_1 (LO) modes are strongly affected by defects (oxygen vacancy or zinc interstitial or their complexes) and/or impurities [17,20].

Table 2
Parameters for Mg-doped ZnO calculated from X-ray diffraction patterns.

Annealing temperature (°C)	Lattice parameter, a (Å)	Lattice parameter, c (Å)	Crystallite size (nm)
700	3.2507	5.2068	38.7
900	3.2439	5.1930	41.0
1100	3.2388	5.1806	43.8

The positions, FWHMs along with possible assignments of the first- and second-order Raman modes are listed in Table 3. The results show good agreement with the previous works where the Raman spectrum of hexagonal ZnO powder was analyzed [17,21].

Exclusively, Fig. 6 shows the plots of half-widths vs. annealing temperature for the E_2^{high} and E_1(LO) modes. As E_2^{high} represents the band characteristic of the wurtzite phase its broadening indicates a change in band structure [22]. This is in acordance with the observed band edge absorption behavior. Increase in half-width of E_1 (LO) (as well as intensity and area, Table 3, Fig. 4) indicates the increase of defects including: V_O^+, V_O^{++} and O_i (oxygen vacancies and interstitials) [23] with the increase of the annealing tempearture. This fits well with the above mentioned progress of the Moss–Burstein effect when intensified diffusion processes between Mg-doped ZnO particles at higher temperatures initiate more Mg replacement of Zn in ZnO tetrahedral coordination instead of the interstitial Mg formation. The Moss–Burstain effect leads to the oxygen vacancies increase that was observed in diffuse reflectance (blue shift of the optical band gap values, Table 1) measurements as well.

3.2. SEM and textural analysis

Results obtained by mercury intrusion porosimetry are summarized in Table 4. As can been seen, total mercury intrusion volume and specific surface area of samples decreased with the increase of the temperature of sample annealed. Also, the mention parameters of Mg-doped ZnO are higher than of pure ZnO on 700 °C and 900 °C of sample annealed. However, V_{tot} and SSA of Mg-doped ZnO and pure ZnO on 1100 °C have similar values. SEM micrographs in Fig. 7a and c show uniform particle size distribution of pure ZnO and Mg-doped ZnO samples annealed at 700 °C, with smaller average grain size of Mg-doped ZnO (~176 nm) compared to ZnO (~330 nm) (Fig. 7d and b). Obviously, SEM results are in accordance with the mercury porosimetry analysis

Table 3
Fitting parameters of Raman modes for Mg-doped ZnO samples and their possible assignments. Numbers in brackets denote the FWHM.

Process [17]	Peak center and FWHM (cm^{-1})		
	Mg-doped ZnO, 700 °C	Mg-doped ZnO, 900 °C	Mg-doped ZnO, 1100 °C
$E_2^{high}-E_2^{low}$	324.2 (31.1)	324.6 (23.5)	323.7 (46.6)
	360.4 (18.8)	360.5 (21.2)	357.9 (16.5)
A_1 (TO)	376.2 (18.2)	376.7 (17.2)	375.6 (29.8)
E_1 (TO)	412.4 (25.9)	414.7 (32.8)	412.2 (32.7)
E_2^{high}	434.8 (9.0)	434.6 (11.9)	434.9 (14.9)
	463.9 (12.5)	463.0 (15.3)	459.5 (3.7)
2LA	486.7 (5.9)	485.7 (10.8)	487.4 (0.00008)
	515.1 (41.2)	512.6 (43.1)	514.5 (22.6)
$2B_1^{low}$; 2LA	544.4 (55.7)	543.9 (55.7)	536.9 (60.9)
E_1 (LO)	584.8 (56.2)	583.6 (58.4)	584.7 (63.2)
TA+TO	619.7 (56.9)	619.3 (56.6)	620.5 (58.6)
TA+LO	662.2 (52.3)	662.1 (53.7)	662.8 (52.2)
LA+TO	697.5 (50.1)	698.6 (47.8)	698.5 (52.5)
2TO	1009.9 (25.7)	1005.4 (44.2)	1006.2 (128.1)
2LO	1094.4 (99.1)	1098.9 (87.6)	1100.4 (83.1)
$2A_1$(LO), $2E_1$(LO); 2LO	1151.9 (83.1)	1153.9 (63.4)	1156.0 (56.5)

(Table 4) showing that Mg-doping improves the textural properties. The bulk density values increase with the increase of the annealing temperature (Table 4) which again agrees with SEM (Fig. 8a–c) where an insight to the Mg-doped ZnO samples' morphology evolution with annealing temperature increase is presented. The process of crystalline growth and rearrangement of grains in powder occur as particles become exposed to intensified diffusion (zinc oxide diffusion becomes significant at temperatures higher than 800 °C [24]). On the account of vacancies reduction the larger grains are formed in the process similar to sintering (Fig. 8c) causing the observed bulk density enhancement.

3.3. Photocatalysis

The photocatalytic degradation kinetics of alprazolam in the presence of the obtained Mg-doped ZnO nanoparticles, pure ZnO and the most frequently used oxide semiconductor for photodegradation (TiO_2 Degussa P25) under UV light irradiation is shown in Fig. 9. The best photocatalytic activity was found for Mg-doped ZnO sample annealed at 700 °C, even better than Degussa P25. Commonly, the photocatalytic activity of an oxide semiconductor is closely related to its particle size, morphology and surface properties [25] i.e. preparation conditions, since photocatalytic reactions mainly occur on the catalyst surface [1]. The efficiency in alprazolam degradation is decreased with the increase of annealing temperature due to deterioration of the textural properties but is improved evidently with Mg-doping especially at temperatures ≤900 °C as the specific surface area (Table 4) of the photocatalyst is higher.

Table 4
Results obtained from mercury intrusion porosimetry.

Sample	V_{tot} (mm^3/g)	SSA (m^2/g)	ρ_{bl} (g/cm^3)
ZnO, 700 °C	363	4.23	1.812
ZnO, 900 °C	160	1.45	3.048
ZnO, 1100 °C	90	0.77	3.804
Mg-doped ZnO, 700 °C	537	5.97	1.398
Mg-doped ZnO, 900 °C	252	3.93	2.366
Mg-doped ZnO, 1100 °C	76	0.92	3.854

V_{tot}—total mercury intrusion volume; SSA—specific surface area; and ρ_{bl}—bulk density.

4. Conclusions

In this paper, we report the structural and optical changes in the ZnO nanoparticles induced by the preparation procedure and Mg-doping and its impact on its photocatalytic efficiency in alprazolam degradation. The Mg-doped ZnO photocatalyst prepared at temperature 700 °C appeared to be most efficient. At higher temperatures (≥900 °C) the inferior photocatalytic activity of Mg-doped ZnO catalyst is a consequence of the grain growth, changed morphology and surface reduction in samples. The substitutional Mg-doping mechanism at high temperatures caused by intensified diffusion, and its expected positive influence on ZnO electronic structure and improved photocatalytic activity, it is unfortunately suppressed by pure textural properties of the Mg-doped ZnO catalyst created when prepared at temperatures ≥900 °C.

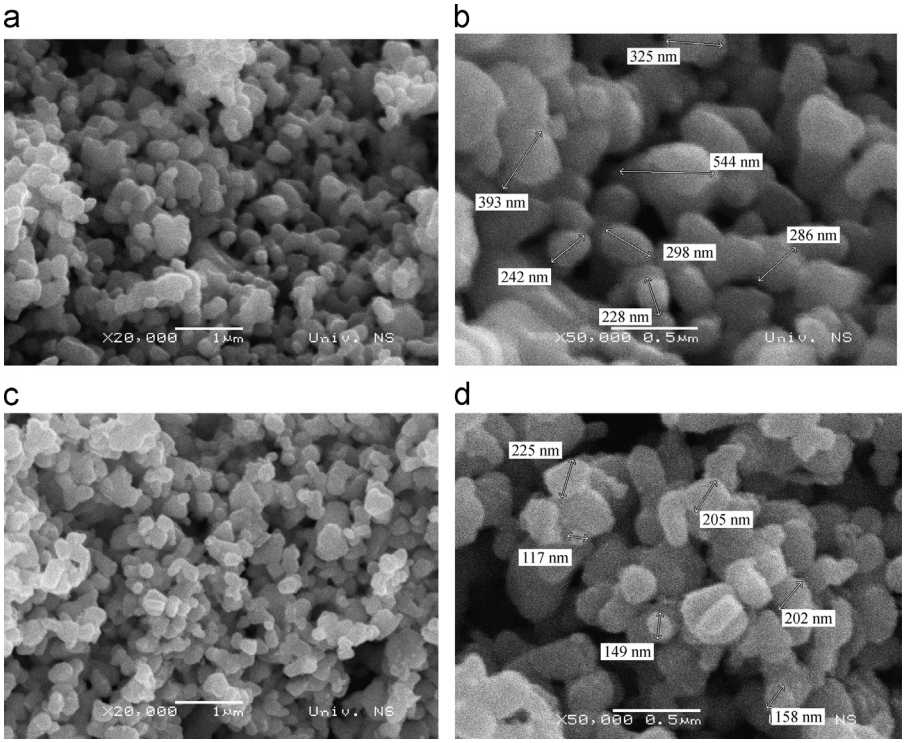

Fig. 7. SEM image of samples annealed at 700 °C: (a) pure ZnO-enlargement × 20,000; (b) pure ZnO-enlargement × 50,000; (c) Mg-doped ZnO-enlargement × 20,000 and (c) Mg-doped ZnO-enlargement × 50,000.

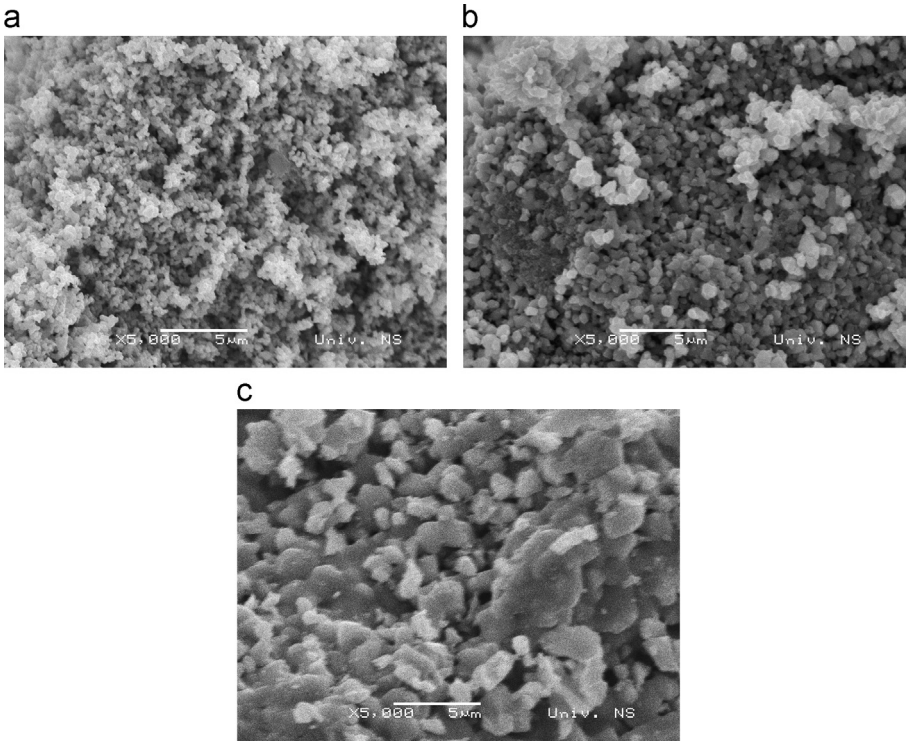

Fig. 8. SEM images of Mg-doped ZnO sample annealed at (a) 700 °C; (b) 900 °C and (c) 1100 °C.

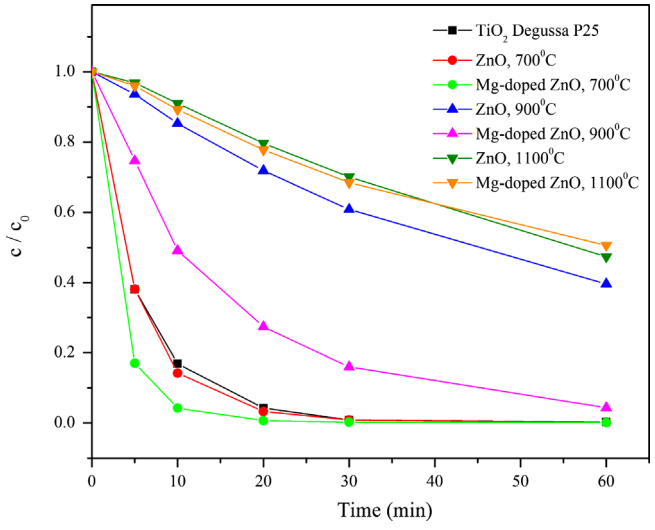

Fig. 9. The kinetics of photocatalytic degradation of alprazolam (c_0=0.03 mmol/L) in the presence of ZnO, Mg-doped ZnO and TiO_2 Degussa P25 (1.0 mg/mL).

Acknowledgments

The authors are grateful to APV Provincial Secretariat for Science and Technological Development of the Republic of Serbia for financing this work, and acknowledge the support of the Ministry of Education, Science and Technological Development of the Republic of Serbia (Projects' nos.: ON 171022, III 45020 and ON 172042).

References

[1] V. Etacheri, R. Roshan, V. Kumar, Mg-doped ZnO nanoparticles for efficient sunlight-driven photocatalysis, ACS Applied Materials and Interfaces 4 (2012) 2717–2725.
[2] P. Kumar, J.P. Singh, Y. Kumar, A. Gaur, H.K. Malik, K. Asokan, Investigation of phase segregation in $Zn_{1-x}Mg_xO$ systems, Current Applied Physics 12 (2012) 1166–1172.
[3] C.-J. Pan, K.-F. Lin, W.-T. Hsu, W.-F. Hsieh, Raman study of alloy potential fluctuations in $Mg_xZn_{1-x}O$ nanopowders, Journal of Physics: Condensed Matter 19 (2007) 186201 (8 pp.).
[4] X. Lu, Z. Liu, Y. Zhu, L. Jiang, Sonochemical synthesis and photocatalytic property of zinc oxide nanoparticles doped with magnesium (II), Materials Research Bulletin 46 (2011) 1638–1641.
[5] V. Calisto, V.I. Esteves, Psychiatric pharmaceuticals in the environment, Chemosphere 77 (2009) 1257–1274.
[6] V. Calisto, M.R.M. Domingues, V.I. Esteves, Photodegradation of psychiatric pharmaceuticals in aquatic environments—kinetics and photodegradation products, Water Research 45 (2011) 6097–6106.
[7] P. Pérez-Lozano, E. García-Montoya, A. Orriols, M. Miñarro, J.R. Ticó, J.M. Suñé-Negre, Development and validation of new HPLC analytical method for the determination of alprazolam in tablets, Journal of Pharmaceutical and Biomedical Analysis 34 (2004) 979–987.
[8] B. Castañeda, W. Ortiz-Cala, C. Gallardo-Cabrera, N.S. Nudelman, Stability studies of alprazolam tablets: effect of chemical interactions with some excipients in pharmaceutical solid preparations, Journal of Physical Organic Chemistry 22 (2009) 807–814.
[9] M. Šćepanović, B. Abramović, A. Golubović, S. Kler, M. Grujić-Brojčin, Z. Dohčević-Mitrović, B. Babić, B. Matović, Z.V. Popović, Photocatalytic degradation of metoprolol in water suspension of TiO_2 nanopowders prepared using sol–gel route, Journal of Sol–Gel Science and Technology 61 (2012) 390–402.
[10] A.E. Morales, E.S. Mora, U. Pal, Use of diffuse reflectance spectroscopy for optical characterization of un-supported nanostructures, Revista Mexicana de Física S 53 (2007) 18–22.

[11] V. Ischenko, S. Polarz, D. Grote, V. Stavarache, K. Fink, M. Driess, Zinc oxide nanoparticles with defects, Advanced Functional Materials 15 (2005) 1945–1954.
[12] Z. Li, W. Shen, S. Xue, X. Zu, Effect of annealing temperature on the structural and optical properties of $Zn_{1-x}Mg_xO$ particles prepared by oxalate precursor, Colloids and Surfaces A 320 (2008) 156–160.
[13] B.E. Sernelius, K.-F. Berggren, Z.-C. Jin, I. Hamberg, C.G. Granqvist, Band-gap tailoring of ZnO by means of heavy Al doping, Physical Review B 37 (1988) 10244–10248.
[14] F.K. Shan, B.I. Kim, G.X. Liu, Z.F. Liu, J.Y. Sohn, W.J. Lee, B.C. Shin, Y.S. Yu, Blueshift of near band edge emission in Mg doped ZnO thin films and aging, Journal of Applied Physics 95 (2004) 4772–4776.
[15] P.M. Aneesh, M.K. Jayaraj, Red luminescence from hydrothermally synthesized Eu-doped ZnO nanoparticles under visible excitation, Bulletin of Materials Science 33 (2010) 227–231.
[16] M.J. Lambregts, S. Frank, Application of Vegard's law to mixed cation sodalites: a simple method for determining the stoichiometry, Talanta 62 (2004) 627–630.
[17] R. Cuscó, E. Alarcón-Lladó, J. Ibáñez, L. Artús, Temperature dependence of Raman scattering in ZnO, Physical Review B 75 (2007) 165202-1–165202-11.
[18] S.-S. Lo, D. Huang, C.-H. Tu, D.-J. Jan, Formation and Raman scattering of seed-like ZnO nanostructure, Journal of Raman Spectroscopy 40 (2009) 1694–1697.
[19] M. Ghosh, N. Dilawar, A.K. Bandyopadhyay, A.K. Raychaudhuri, Phonon dynamics of Zn(Mg,Cd)O alloy nanostructures and their phase segregation, Journal of Applied Physics 106 (2009) 084306-1–084306-6.
[20] P.K. Giri, S. Bhattacharyya, D.K. Singh, R. Kesavamoorthy, B.K. Panigrahi, K.G.M. Nair, Correlation between microstructure and optical properties of ZnO nanoparticles synthesized by ball milling, Journal of Applied Physics 102 (2007) 093515-1–093515-8.
[21] T.B. Ivetić, M.R. Dimitrievska, I.O. Gúth, Lj.R. Đačanin, S.R. Lukić-Petrović, Structural and optical properties of europium doped zinc oxide nanopowders prepared via mechanochemical and combustion reaction methods, Journal of Research in Physics 36 (inpress).
[22] Y.-I. Kim, R. Seshadri, Microstrain and defects in polycrystalline $Zn_{1-x}Mg_xO$ ($0 \leq x \leq 0.15$) studied by X-ray diffraction and optical and Raman spectroscopies, Journal of the Korean Physical Society 53 (2008) 2835–2839.
[23] C.-Y. Kung, S.-L. Young, H.-Z. Chen, M.-C. Kao, L. Horng, Y.-T. Shih, C.-C. Lin, T.-T. Lin, C.-J. Ou, Influence of Y-doped induced defects on the optical and magnetic properties of ZnO nanorod arrays prepared by low-temperature hydrothermal process, Nanoscale Research Letters 7 (2012) 372-1–372-6.
[24] A.A. Letailleur, S.Y. Grachev, E. Barthel, E. Søndergård, K. Nomenyo, C. Couteau, S. Mc Murtry, G. Lérondel, E. Charlet, E. Peter, High efficiency white luminescence of alumina doped ZnO, Journal of Luminescence 131 (2011) 2646–2651.
[25] X. Qiu, L. Li, J. Zheng, J. Liu, X. Sun, G. Li, Origin of the enhanced photocatalytic activities of semiconductors: a case study of ZnO doped with Mg^{2+}, Journal of Physical Chemistry C 112 (2008) 12242–12248.